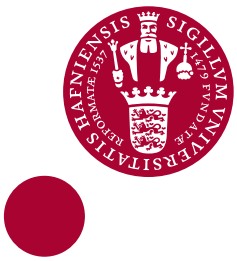

Insulin fibrillation

The influence and coordination of Zn2+

Frankær, Christian Grundahl; Sønderby, Pernille; Bang, Maria Blanner; Mateiu, Ramona Valentina; Groenning, Minna; Bukrinski, Jens; Harris, Pernille

Published in:
Journal of Structural Biology

DOI:
10.1016/j.jsb.2017.05.006

Publication date:
2017

Document version
Peer reviewed version

Insulin Fibrillation: The Influence and Coordination of Zn^{2+}

Christian Grundahl Frankær[a], Pernille Sønderby[a], Maria Blanner Bang[a], Ramona Valentina Mateiu[b] , Minna Groenning[c, 1], Jens Bukrinski[d], and Pernille Harris[a]*

[a]Department of Chemistry, Technical University of Denmark, Kgs. Lyngby, Denmark

[b]Department of Physics, Technical University of Denmark, Kgs. Lyngby, Denmark

[c]Department of Pharmaceutics and Analytical Chemistry, Faculty of Pharmaceutical Sciences, University of Copenhagen, DK-2100 Copenhagen, Denmark[1]

[d]CMCassist ApS, Copenhagen, Denmark

*Corresponding author. E-mail: ph@kemi.dtu.dk

Insulin – Fibrillation – Amyloid – Zinc – Thioflavin T – XAS – EXAFS – Fiber diffraction – TEM

Abbreviations

EXAFS – Extended X-ray absorption fine-structure

SAXS – Small-angle X-ray scattering

ThT – Thioflavin T

XANES – X-ray absorption near-edge structure

XAS - X-ray absorption spectroscopy

Abstract:

Protein amyloid fibrillation is obtaining much focus because it is connected with amyloid-related human diseases such as Alzheimer's disease, diabetes mellitus type 2, or Parkinson's disease. The influence of metal ions on the fibrillation process and whether it is implemented in the amyloid fibrils has been debated for some years. We have therefore investigated the influence and binding geometry of zinc in fibrillated insulin using extended X-ray

[1] Present address: Novo Nordisk A/S, Måløv, Denmark

absorption fine-structure and X-ray absorption near-edge structure spectroscopy. The results were validated with fiber diffraction, Transmission Electron Microscopy and Thioflavin T fluorescence measurements. It is well-known that Zn^{2+} ions coordinate and stabilize the hexameric forms of insulin. However, this study is the first to show that zinc indeed binds to the insulin fibrils. Furthermore, zinc influences the kinetics and the morphology of the fibrils. It also shows that zinc coordinates to histidine residues in an environment, which is similar to the coordination seen in the insulin R_6 hexamers, where three histidine residues and a chloride ion is coordinating the zinc.

Introduction

Protein and peptide amyloid fibrillation is an increasingly significant field of research due to the growing prevalence and recognition of amyloid-related human diseases such as Alzheimer's disease (amyloid-β peptide), diabetes mellitus type 2 (human islet amyloid polypeptide, hIAPP), or Parkinson's disease (α-synuclein protein). The pancreatic hormone insulin is also known to form amyloid-like fibrils; first recognized 70 years ago (Waugh, 1944). In relation to the therapeutic application of insulin, this aggregation phenomenon constitutes a challenge during the production and transportation (Nielsen et al., 2001c), and *in vivo* fibrillation has been observed after both insulin infusion (Storkel et al., 1983) and injection (Dische et al., 1988). From a physiological point of view, insulin fibrillation is highly undesirable because it prevents the important biological purpose of insulin requiring monomer interaction with insulin receptors. In addition, some of the intermediate prefibrillar oligomers might even be cytotoxic or immunogenic (Noormägi et al., 2010).

Insulin fibrillation represents a good system for fibril studies in general. Monomeric insulin is a small (51 residues) globular protein hormone (Groenning et al., 2009), not considered dangerous (Nayak et al., 2009), commercially available at a relatively low cost, and well-studied. It should be noted, however, that insulin differs from other amyloidogenic proteins regarding the effect of protein concentration: at physiological pH insulin is more susceptible to fibrillation at *lower* insulin concentration (J Brange et al., 1997; Groenning et al., 2009; Noormägi et al., 2010).

The formation of insulin fibrils is typically measured using the dye Thioflavin T (ThT) (Groenning, 2010).When fibrils are developed, they interact with ThT and change the fluorescence signal: enhanced emission at 482 nm and a new excitation maximum at 450 nm are observed (Levine, 1995, 1993). Essentially, detection of fibril formation with the ThT fluorescence assay gives rise to a sigmoidal curve comprising a nucleation phase defined by the lag time, an elongation phase defined by the rate constant, and an equilibrium phase (Nielsen et al., 2001c). The fibrillation kinetics is affected by various factors such as insulin concentration, pH, temperature, agitation, different ions and additives, as well as ionic strength (Nielsen et al., 2001c; Noormägi et al., 2010).

Numerous pathways of insulin fibrillation have been suggested (Ahmad et al., 2004, 2003; Krebs et al., 2008; Librizzi and Rischel, 2005; Nayak et al., 2009; Nielsen et al., 2001c; Podestà et al., 2006; Sluzky et al., 1991) (and others). In general, partially unfolded insulin monomers (or dimers) are believed to be a vital prerequisite for prefibrillar oligomerization and eventually fibril formation (reviewed by Groenning *et al.* (Groenning et al., 2009)).

Zn^{2+} ions coordinate and stabilize the hexameric forms of insulin. In the T_6 hexameric conformation, both Zn^{2+} sites are octahedral and coordinated by three symmetry-related histidine imidazole rings (HisB10) as well as three symmetry-related water molecules (Baker et al., 1988; Bordas et al., 1983; Frankær et al., 2012; Kaarsholm et al., 1989; Smith et al., 2005, 2003). The R_6 hexameric conformation has a tighter tetrahedral coordination around the Zn^{2+} ions comprising the three HisB10 residues and a lyotopic anion such as chloride (Frankær et al., 2012). Finally, in the T_3R_3 hexameric conformation, both the octahedral and the tetrahedral coordination geometry are present (Ciszak and Smith, 1994; Frankær et al., 2012; Kaarsholm et al., 1989).

As fibrillation is commonly found to occur from the biologically active, monomeric form of insulin, zinc is considered to impede insulin fibril formation through stabilization of the physiological predominant hexameric forms (Andra et al., 2010; Brange et al., 1986; J Brange et al., 1997). Hence, pharmaceutical formulations of insulin usually include well-considered equivalents of zinc (Jens Brange et al., 1997b). However, the question arises whether the assigned monomeric pathway at least to some degree could be a premise generated from the usual experimental procedure of inducing fibril formation; that zinc is avoided in the insulin samples, or that experiments are conducted at acidic conditions with protonated histidine residues that cannot coordinate the Zn^{2+} ions, in order to induce the monomeric form believed to be the prerequisite of insulin fibrillation? In a more recent study by Noormägi *et al.* (Noormägi et al., 2010), it was suggested that Zn^{2+} ions also inhibit fibrillation though differential stabilization of the insulin monomer.

hIAPP is produced and stored in the β-islet cells in pancreas together with insulin. Interestingly, amyloid fibrillation of hIAPP has been found to be dependent on the presence of metal ions, such as zinc or copper that have the ability to coordinate histidine (Brender et al., 2010). An extensive study characterizing the structure of hIAPP using NMR shows that zinc is coordinating a histidine and thereby inducing a kink in the alpha-helical structure of hIAPP (Brender et al., 2010; Patel et al., 2014). Zinc which is found in mM concentrations in the islet cells inhibit at these concentrations amyloid fibrillogenisis both by increasing the lag-time and decreasing the fibril growth rate. At higher hIAPP concentrations zinc is found to have the opposite effect.

To our knowledge, nobody has looked for zinc binding in insulin fibrillation. We therefore set out to see if we could establish whether zinc would bind to the fibrils at physiological pH or not.

In the present work, we have therefore investigated the presence and influence of zinc at well-defined stoichiometric levels, as well as the inner coordination sphere of Zn^{2+} during insulin fibril formation, using X-ray absorption spectroscopy (XAS) including both extended X-ray absorption fine-structure (EXAFS) and X-ray absorption near-edge structure (XANES) spectroscopy. Characteristic EXAFS ‘fingerprints’ of the different zinc coordination geometries of hexameric bovine insulin have recently been identified (Frankær et al., 2012) and were

used for analysis of the present data. In addition, the results were validated with fiber diffraction, TEM and fluorescence measurements.

Material and Methods

Lyophilized insulin from bovine pancreas, *Bos taurus*, was purchased from Sigma Aldrich (I-5500). Other reagents used were stock chemicals, biological grade. All solutions were prepared in fresh Milli-Q water and filtered using a 0.22 µm filter press.

Preparation of insulin samples for fibrillation

Metal-free insulin was prepared by chelating using the method of Coffman & Dunn(Coffman and Dunn, 1988). After chelation the supernatant was separated from the resin by syringe filtration (0.22 µm). The protein concentration was determined by UV-vis spectrophotometry using an extinction coefficient at 280 nm, ε_{280}, of 5960 $M^{-1}cm^{-1}$, as estimated by *ProtParam* (Gasteiger et al., 2005) tool from *ExPASy* (Gasteiger, 2003). Hereafter, samples were prepared by adding stoichiometric amounts of $ZnCl_2$ (two Zn atoms per six insulins) using a buffer of 100 mM NaCl, 20 mM Hepes, pH 7.3, and (if the samples were to be monitored by fluorescence measurements) 20 µM thioflavin T (ThT). Zn free samples were prepared analogously, but without addition of $ZnCl_2$.

Fibrillation of insulin

Insulin samples were prepared with and without $ZnCl_2$ added and at insulin concentrations of 10.0, 2.0, 0.2 and 0.02 mg ml^{-1}. In order to eliminate the effect of ThT on the binding of Zn-ions, samples with $ZnCl_2$ added but without ThT were also prepared. All final preparations were filtered on a 0.22 µm filter before experiments.

Portions of 100 µL protein samples were fibrillated at temperatures varying between 35 and 55 ºC in a Fluostar Optima plate reader from BMG Labtechnologies. Agitation was performed in double orbital mode with a speed of 600 rpm for 150 s every 5 minutes. The increase in ThT fluorescence was measured at 490 nm. At least 10 replicates were done for each sample. Samples to be used in the XAS experiments were fibrillated at 45 ºC and removed after 6 hours and 14 hours for semi-matured and matured samples, respectively.

X-ray scattering: Fibre diffraction and SAXS

Samples were taken directly from the preparation on the Fluostar Optima plate reader after full maturation. They were centrifuged at 18,000 *g* and dried in a desiccator. X-ray fibre diffraction data were collected using an Agilent Supernova diffractometer with Cu-Kα radiation (λ = 1.5418 Å) using 60 s exposure time.

The metal-free insulin was dialyzed against 3×1 l buffer containing 100 mM NaCl, 20 mM Hepes, pH 7.3. Concentration determinations were performed with the NanoDrop® 1000 Spectrophotometer from Thermo Scientific at 280 nm using the extinction coefficient ε_{280}, of 5960 $M^{-1}cm^{-1}$, as mentioned above. Stoichiometric amounts of $ZnCl_2$ (two zinc ions per six insulins) were added to the Zn-containing samples, but not to the buffer.

SAXS measurements were performed at the MAX IV laboratories at beamline I911-SAXS (Labrador et al., 2013), Sweden (see Table 1). The sample detector distance and the direct beam position was calibrated using silver behenate (AgBe). Measurements on pure water were used to get the data on an absolute scale. Buffers were measured both before and after each sample and averaged before subtraction. The sample size was approximately 50 µl injected manually in a flow cell. Measurements were performed on two series of insulin samples – with and without $ZnCl_2$ added – at approximate concentrations of insulin: 1, 2, 5, 7 and 10 mg ml^{-1}.

Table 1: Experimental set up of SAXS measurements.

Instrument	MaxIV beamline I911-SAXS
Detector	PILATUS 1M
Wavelength (Å)	0.9100
q range (nm)	0.08-4.8
Exposure time (s)	5×30
Temperature (K)	298
Sample–detector distance (mm)	2001

Calibrations and corrections of the data were done using the in-house software Bli911-4(Labrador et al., 2013). Buffer averaging and subsequent subtraction prior to data analysis was done in *Primus*(Konarev et al., 2003). The *ATSAS* program package version 2.4(Petoukhov et al., 2012) was used for further data analysis. To estimate the volume fractions the dimeric insulin structure from PDB-entry 1B17(Diao, 2003) (zinc free) was used to estimate the dimer while PDB-entry 1MSO(Smith et al., 2003) (T-state) was used to produce pdb files of hexamer and dodecamer as higher order species are present. *FFMAKER* (Konarev et al., 2003) was used to produce a formfactor file using *Crysol* (Svergun et al., 1995). This information was then utilized in the program *Oligomer* (Konarev et al., 2003) to estimate the volume fractions.

Transmission electron microscopy

The fibers were imaged in an FEI Tecnai T20G^2 transmission electron microscope. All samples were mounted onto an 200 mesh Formvar Carbon film Cu grid, which was made hydrophilic in an Cressington oxygen/argon plasma, and negative stained with 2 % aqueous solution uranyl acetate, as described. On a piece of parafilm one droplet of sample was placed followed by 3 droplets of milli-Q water, a droplet of stain and another 3 droplets of milli-Q water. The grid was placed on the sample for 1 min, washed 3 times in the milli-Q water, stained for 1 min and washed again 3 times in milli-Q water, followed by drying with filter paper. The TEM was operated at 200 keV.

X-ray absorption spectroscopy

X-ray absorption spectra were collected at the Zn *K*-edge at the synchrotron MAX II at MAXIV Laboratories, Lund, Sweden on beamline I811 (Carlson et al., 2006) using a Si(111) double-crystal monochromator detuned 60% at 10510 eV. The fibrillated protein samples were isolated by filtration using an Ultra-free-MC centrifuge filter (Amicon/Millipore) with a pore size of 0.22 µm, washed 3 times in 500 µl zinc free buffer of 100 mM NaCl and 20 mM Hepes, pH 7.3. The isolated samples were mounted in 1 mm thick sample holders (Frankr et al., 2011), and cooled to 100 K in a cryostat using liquid nitrogen. Fluorescence data were collected using a PIPS PD-5000 (Passivated Implanted Planar Silicon) detector from Canberra equipped with Soller slits and a copper filter to suppress non-Zn fluorescence scattering. Data were collected in the region 9510–10510 eV in similar intervals as described by Frankær *et al.* (Frankær et al., 2012).

XAS spectra were measured on isolated insulin fibril preparations sampled from the fibrillation series after approximately 50 % maturation (semi-matured) and after full maturation. This included samples with and without ThT, and with insulin concentrations of both 2 and 10 mg ml^{-1} insulin. ThT did not have any influence on the XAS spectra. The spectra collected for the two different insulin concentrations were similar, but owing to the higher zinc content, the high insulin concentration samples gave better signal-to-noise ratios. Therefore, only 10 mg ml^{-1} preparations of respectively fully matured insulin fibrils and semi-matured fibrils are presented in the following. Five spectra were recorded on the fully matured fibril sample and three spectra were recorded on the semi-matured fibril sample to ensure reproducibility and that no radiation damage of the samples had taken place.

The data reduction was carried out using *WinXAS* (Ressler, 1998) where the EXAFS function $\chi(k)$ was extracted after deglitching, averaging, energy calibration and background subtraction of the spectra. The following EXAFS analysis was carried out using *EXCURVE* (Binsted et al., 1991; Gurman et al., 1986, 1984). The atomic models tested were refined by a constrained refinement, where each ligand was assumed to be rigid and refined by only one distance and one angular parameter (Binsted et al., 1992). Furthermore Debye-Waller factors of atoms with similar distances to the central atom were grouped in order to keep the number of refined parameters to a minimum.

Data evaluation of fibrillation kinetics

The kinetics of the fibrillation is followed by change in ThT fluorescence intensity. The fibrillation of insulin generally results in sigmoidal curves. After an initial lag phase the fibrillation subsequently enters a sigmoidal growth phase in which the growth rate is characterized by the apparent rate constant k_{app} as described by Nielsen *et al.* (Nielsen et al., 2001c) Hereafter it finalizes at a plateau where equilibrium is obtained. In some samples fluorescence decay was observed after the finalization. These data have been rejected or truncated.

The fibrillation process of insulin in presence of stoichiometric zinc showed higher variations and was generally less reproducible compared to the Zn-free samples. Different models were tested to describe these features. It was found that the following simple sigmoidal models provided the best fitting of the overall fibrillation curve. The single step model was used to evaluate the fibrillation rate of the overall process for all samples reported here:

$$Y(t) = \frac{1}{\left(1+e^{\frac{-(t-t_0)}{\tau}}\right)},$$

in which $Y(t)$ is the percentage insulin fibrillated (i.e. the normalized fluorescence signal), t_0 is the time were the fibrillation has come to 50% completion, and $1/\tau$ is the apparent rate constant k_{app}. The lag time t_{lag} was approximated as $t_0–2\tau$ according to Nielsen *et al.*(Nielsen et al., 2001c). However, in some experiments a two-step curve was observed giving rise to the following double step model in which two elongation phases are present:

$$Y(t) = \frac{x}{\left(1+e^{\frac{-(t-t_{0,1})}{\tau_1}}\right)} + \frac{1-x}{\left(1+e^{\frac{-(t-t_{0,2})}{\tau_2}}\right)},$$

x is the fraction of insulin fibrillated in the first elongation step, $t_{0,1}$ and $t_{0,2}$ are the times were the fibrillation has come to 50% completion in the two elongation phases, respectively, and $1/\tau_1$ and $1/\tau_2$ are the apparent rate constants $k_{app,1}$ and $k_{app,2}$ for the first and second elongation phase, respectively. The lag time t_{lag} was approximated as $t_{0,1}–2\tau_1$ according to Nielsen *et al.*(Nielsen et al., 2001c). The model fitting was performed in Matlab.

The temperature dependence on fibrillation was studied at insulin concentrations of 2.0, 0.2 and 0.02 mg ml^{-1}, and was evaluated by an Arrhenius plot from which the activation energy was estimated. The measured average and standard deviation of k_{app} for each sample were used to generate 3000 data points from a normal distribution. The error estimation of the activation energy was subsequently calculated from linear regression of each of the 3000 sets of generated data points.

Results

X-ray scattering experiments: Fibre diffraction and SAXS

The fibre diffraction patterns for fibrils fibrillated in both absence and presence of Zn at pH 7.3 and at pH 2.0 are presented in Figure 1. The fibrillated samples were transferred to Eppendorf tubes and left to dry out overnight. In all three samples diffraction is seen as a fairly strong signal at 4.7 Å indicating the presence of β-strands creating a β-sheet, and as a weaker and more diffuse signal around 11.7–9 Å, normally assigned as originating from the stacking of β-sheets and thereby demonstrating that fibrils are formed. It is clear from the three diffraction patterns that the alignment of the fibers is higher in Figure 1a and 1c, while the diffraction in Fig. 1b indicate disordered orientations.

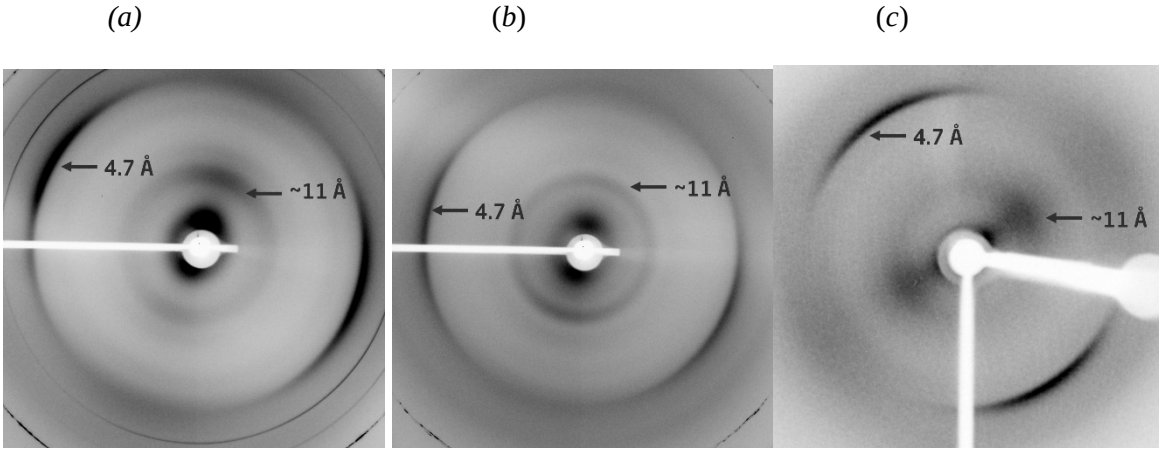

Figure 1: Fibre diffraction images from fibrils fibrillated from 2 mg ml^{-1} insulin at 45°C. (*a*) Zn-free fibrils, pH 7.3. (*b*) Fibrils fibrillated in presence of stoichiometric Zn^{2+}, pH 7.3, (*c*) Fibrils fibrillated at pH 2.0 (0.1 M HCl).

.

The SAXS experiments performed from 1 to 10 mg/mL showed that the zinc-free samples have a concentration dependent equilibrium between the different oligomers. They appear to be predominantly dimers at low concentrations – with a fraction of hexamers depending on the concentration and with higher oligomers appearing and dominating at higher concentrations. The zinc-containing samples are predominantly hexameric, and comparison with calculated SAXS curves for the different insulin hexamer conformations clearly demonstrates that the hexamers adopt T_6 conformation. The experiments cannot be performed at 0.02 and 0.2 mg/mL why we can only extrapolate. The experimental SAXS results are shown in Table. 2.

Table 2: SAXS determination of the contents of the samples at the initial stage – i.e. before fibrillation was performed.

	Zn-free samples			Zn containing samples	
Concentration (mg/mL)	Fraction of dimer (%)	Fraction of hexamer (%)	Fraction of higher oligomers(%)	Fraction of dimer (%)	Fraction of hexamer (%)
1.0	77	16	7	0	100
2.0	72	12	16	0	100
5.0	63	0	37	0	100
7.0	53	0	47	0	100
10.0	51	0	49	0	100

Transmission electron microscopy

Representative TEM images of insulin fibrils fibrillated in absence and presence of Zn^{2+} are presented in Figure 2. The fibrils showed a surprising morphology compared to previous reported TEM studies of fibrils made at lower pH. To our surprise a lumpy morphology was observed, which was first believed to be aggregates. To confirm this morphology TEM images were taken of a reference sample fibrillated 0.1 M NaCl at pH 2, Figure 2(*c*), showing elongated fibrils that highly resemble previous studies (Domigan et al., 2012; Kurouski et al., 2012; Nielsen et al., 2001b). Also samples without ThT were prepared eliminating the possibility of ThT precipitation.

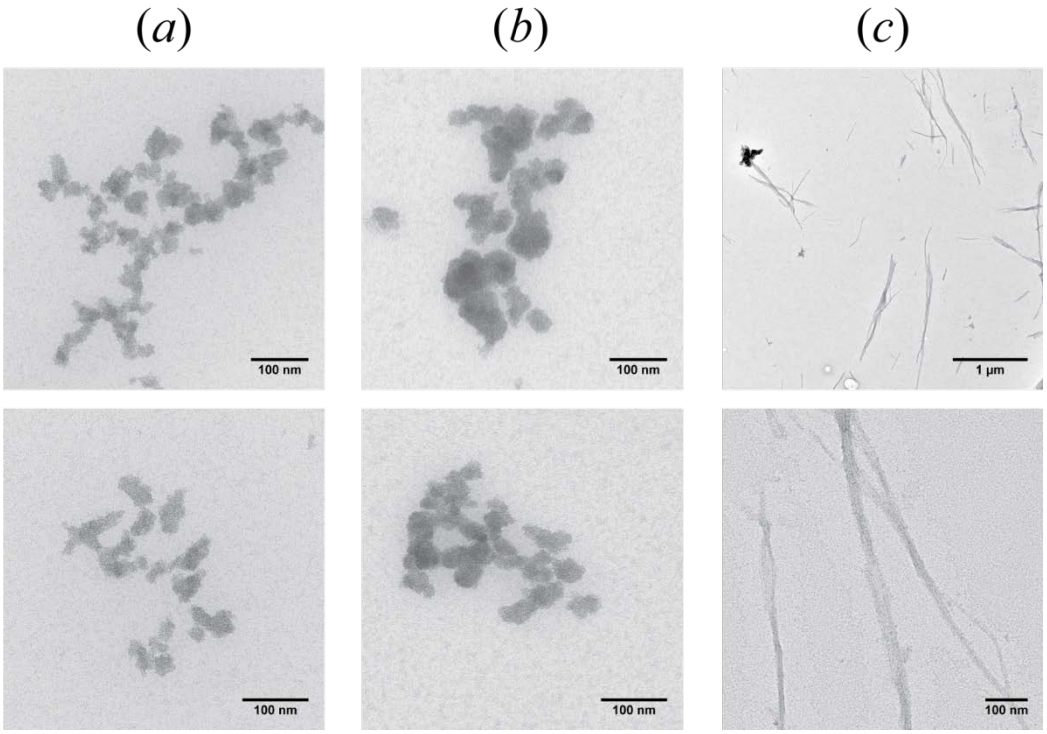

Figure 2: TEM images from fibrils fibrillated from 2 mg ml^{-1} insulin at 45°C. (*a*) Zn-free fibrils, pH 7.3. (*b*) Fibrils fibrillated in presence of stoichiometric Zn^{2+}, pH 7.3 (*c*) Zn-free fibrils, pH 2.0. Two representative images are shown for each sample. Scale bar is 100 nm, except for upper (*c*), where it is 500 nm.

At pH 7.3, the morphology of the fibrils shows several similarities independent of presence of zinc. A size distribution was calculated from a series of TEM images and presented in Figure 3. The size distribution was modelled by a log-normal function and statistics and fitting parameters are presented in Table 3. According to the size distribution, the fibrils are slightly larger when fibrillated in presence of zinc, and they tend to be slightly less frayed compared to the Zn-free.

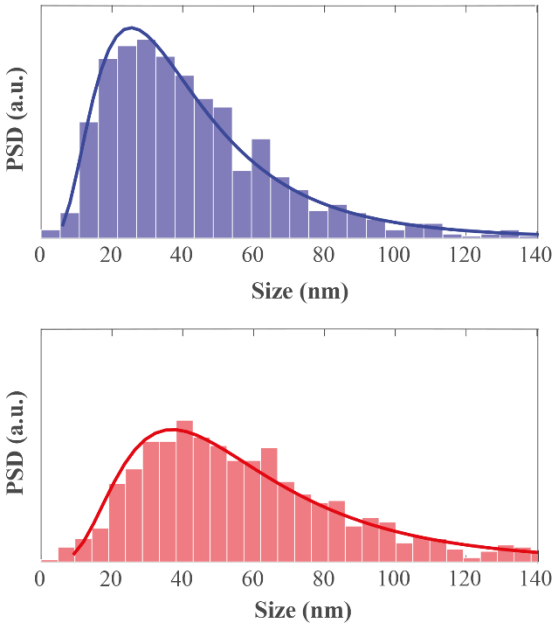

Figure 3: Size distribution (PSD: Particle Density Function) of insulin fibrils fibrillated at pH 7.3 in absence of zinc (top) and in presence of stoichiometric zinc (bottom).

Table 3: Data statistics and fitting parameters for log-normal size distributions of insulin fibrils fibrillated at pH 7.3.

	Zinc-free samples	Zn-containing samples
No. of TEM images	9	10
No. of distances in data set	846	837
Mean (nm)	44	61
Median (nm)	36	52
Standard deviation (nm)	29	39

X-ray absorption near edge spectroscopy

XANES spectra with normalized edge steps of the semi-matured and the fully matured insulin fibrils are shown in Figure 4(*b*, *c*), while the spectra of crystalline T_6-insulin is shown in Fig. 4(*a*) and of R_6-insulin is shown in Fig. 4(*d*). In the normalized spectra white line intensities well below 1.5, (1.36 and 1.28 for respectively the semi- and the fully matured fibrils) were observed, which demonstrates predominantly four-coordinated zinc species in both samples (Feiters et al., 2003). In the region 9700–9750 eV (corresponding to approximately 4–5 $Å^{-1}$ in *k*-space) a camel-back shaped feature occurs owing to coordination of Zn^{2+} to the imidazole groups from histidine present in insulin (Bordas et al., 1983).

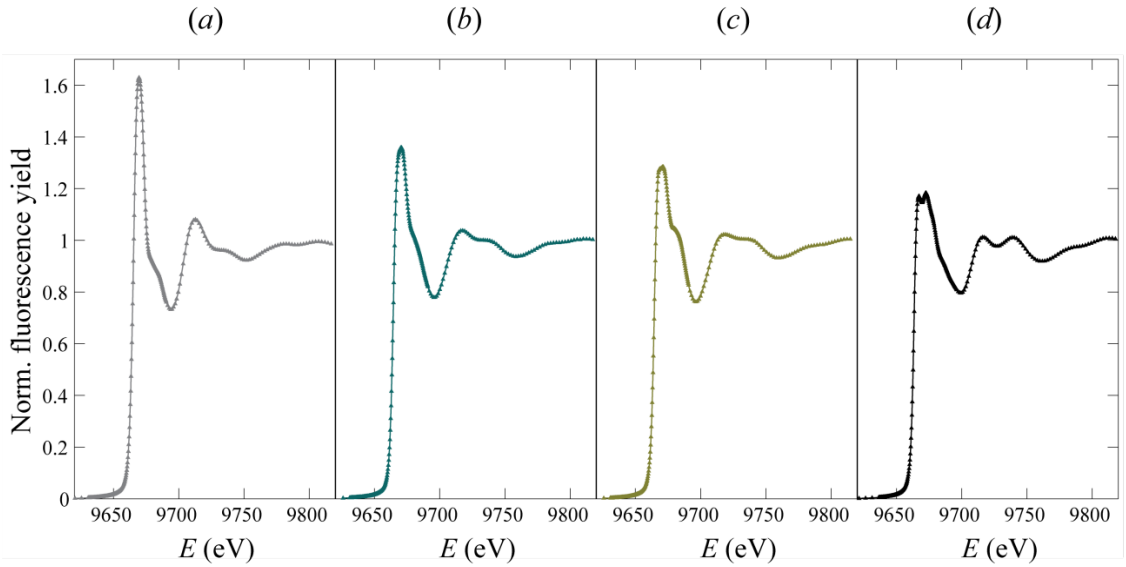

Figure 4: XANES spectra with normalized edge steps for (*a*) crystalline T_6 insulin, (*b*) semi-matured insulin fibrils, (*c*) fully matured insulin fibrils and (*d*) crystalline R_6 insulin. Data from crystalline samples are shown for comparison see description in Frankær *et al.*(Frankær et al., 2012).

The slightly more intense white line observed in the semi-matured fibrils indicate the presence of a minor fraction of octahedrally coordinated zinc which in general give rise to very intense white lines with normalized edge steps around 2.0 (Inada et al., 1999; Zitolo and D'Angelo, 2010).

Generally the absorption spectra of the fibrils have high similarity to the spectrum of R_6-insulin reported by Frankær *et al.* (Frankær et al., 2012), in which Zn^{2+} is coordinated to three histidine residues and one chloride ion. Using a linear combination of XANES spectra for crystalline T_6-insulin (six-coordinated Zn^{2+}) and R_6-insulin (four-coordinated Zn^{2+}) as reported by Frankær *et al.* (Frankær et al., 2012) resulted in 78% tetrahedral and 22% octahedral coordination in the semi-matured fibril sample and 95 % tetrahedral and 5% octahedral coordination in the fully matured fibrils.

Extended X-ray absorption fine structure spectroscopy

The absorption spectra clearly shows that histidine residues in the insulin fibrils are involved in the zinc coordination, which is predominantly four-coordinated, but the number of histidine ligands and geometry cannot be determined solely from qualitative analysis of the spectra. Therefore, we proceeded to compare different geometry-models including 2 or 3 histidine residues, which have been refined to the EXAFS data from the fully matured fibrillated sample.

Table 4: Zn-coordination distances, R, and Debye-Waller factors, $2\sigma^2$, in five different models, as refined by constrained EXAFS refinement for fully matured insulin fibrils. Initial models are taken from the PDB-entries listed. Zn-coordination distances observed in R_6 Zn-insulin crystals by EXAFS (Frankær et al., 2012) have been included for comparison.

Model	(*a*)		(*b*)		(*c*)		(*d*)		(*e*)		R_6 Zn-insulin crystals	
Cluster	$ZnHis_3(H_2O)_3$		$ZnHis_3Cl$		$ZnHis_3(H_2O)$		$ZnHis_2Cl_2$		$ZnHis_2(H_2O)_2$		$ZnHis_3Cl$	
Symmetry	C_3		C_3		C_3		C_2		C_2		C_3	
PDB-entry	4E7T		1EV3		1EV3*		1G7A†		1G7A*†		-	
	R (Å)	$2\sigma^2$ (Å^2)	R (Å)	$2\sigma^2$ (Å^2)	R (Å)	$2\sigma^2$ (Å^2)	R (Å)	$2\sigma^2$ (Å^2)	R (Å)	$2\sigma^2$ (Å^2)	R (Å)	$2\sigma^2$ (Å^2)
$N^{\varepsilon 2}$	1.980(9)	0.008(2)	1.975(4)	0.004(1)	2.00(1)	0.009(2)	1.967(5)	0.002(1)	1.988(8)	0.004(2)	2.001(4)	0.007(1)
$C^{\varepsilon 1}$	2.93‡	0.022(9)	2.90‡	0.025(4)	2.90‡	0.018(15)	2.92‡	0.020(12)	2.98‡	0.019(5)	2.98(2)§	0.010(2)
$C^{\delta 2}$	3.01‡	0.022(9)	3.02‡	0.025(4)	3.06‡	0.018(15)	2.99‡	0.020(12)	2.97‡	0.019(5)	3.04(2)§	0.010(2)
$N^{\delta 1}$	4.06‡	0.030(13)	4.04‡	0.029(6)	4.05‡	0.029(6)	4.04‡	0.017(12)	4.08‡	0.020(9)	4.15(1)§	0.012(2)
C^{γ}	4.13‡	0.030(13)	4.13‡	0.029(6)	4.16‡	0.029(6)	4.11‡	0.017(12)	4.11‡	0.020(9)	4.14(2)§	0.012(2)
C^{β}	5.56‡	0.030(13)	5.56‡	0.029(6)	5.60‡	0.029(6)	5.54‡	0.017(12)	5.53‡	0.020(9)	5.53(3)§	0.012(2)
O^{w}	2.02(2)	0.030(7)			1.94(3)	0.009(7)			1.98(2)	0.018(4)		
Cl			2.25(1)	0.018(3)			2.22(1)	0.027(2)			2.218(3)	0.006(1)
R_{exafs} (%)	26.85		18.23		22.00		19.79		21.80			

*The chlorine atom present in these structures has been substituted by an oxygen atom. †The geometry in these models has been simplified to C_2-symmetry. ‡The rotation angle of the histidine unit around an axis orthogonal to the imidazole plane passing through the $N^{\varepsilon 2}$ atom was included in the refinement. §The presented results are from a restrained refinement in which the positions of all imidazole atoms were refined by refining the φ-angle (polar coordinates). Restrained refinement was only possible due to better EXAFS data for this insulin crystal sample.

In Table 4 refined Zn-coordination distances and Debye-Waller factors are listed for five different models used in the constrained EXAFS refinement using data up to 13.1 Å^{-1} in k-space. The Zn-coordination distances as refined from EXAFS (restrained refinement) for R_6 Zn-insulin crystal and reported by Frankær *et al.*(Frankær et al., 2012)

are included in Table 4 for comparison. The data from the fibrillated samples only allowed for constrained refinement. Restrained refinement strategy was tested on the fibril data as well, but resulted in poorer fits. The calculated EXAFS spectra for the different models have been compared with the experimental spectra in Figure 5.

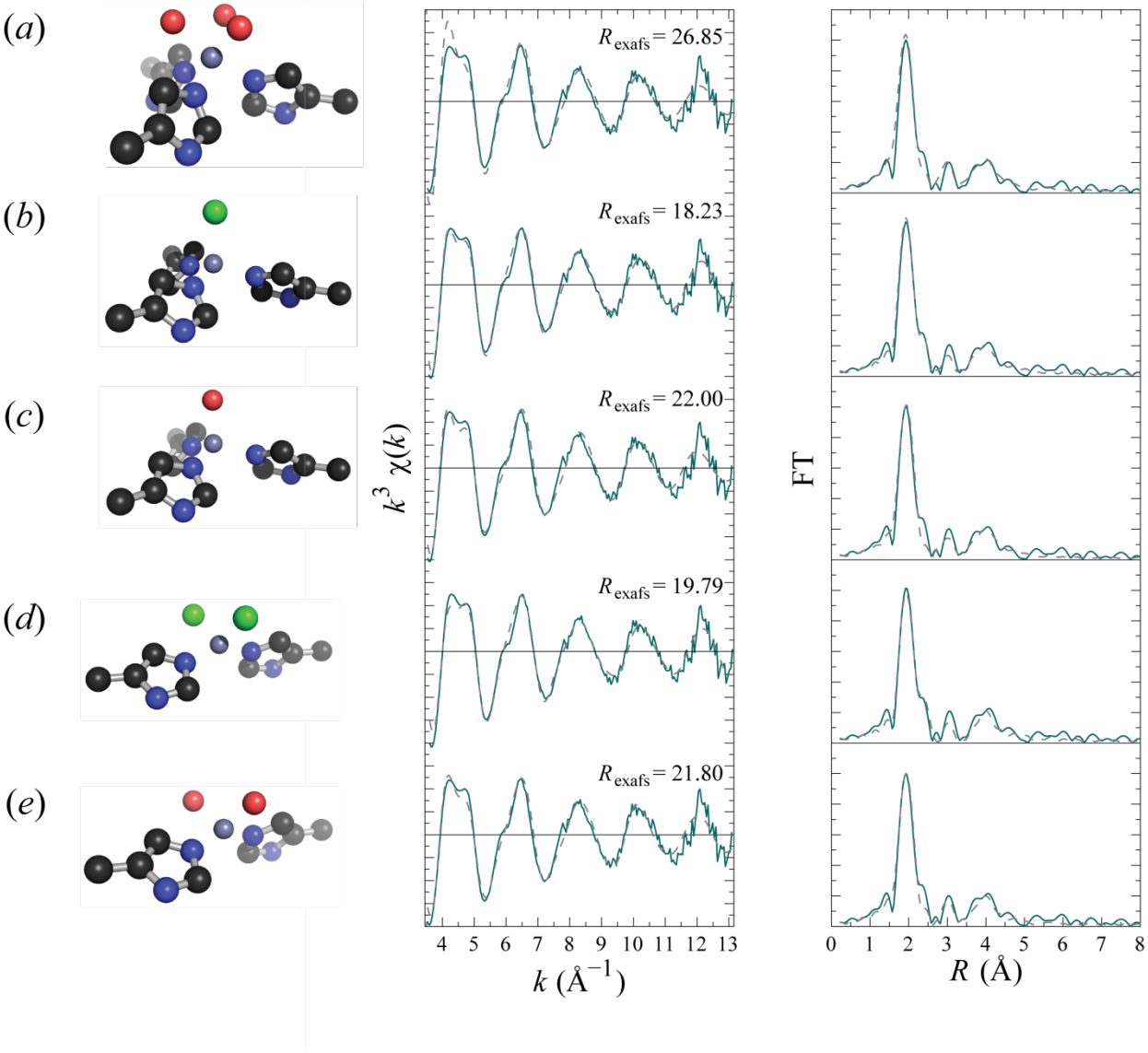

Figure 5: Atomic models (left), k^3-weighted EXAFS spectra (centre), and radial distribution functions calculated as the modulus of the phase-corrected Fourier transform (right) of five different models used in the EXAFS analysis of the fully matured insulin fibrils. (*a*) six-coordinated $ZnHis_3(H_2O)_3$, (*b*) four-coordinated $ZnHis_3Cl$, (*c*) four-coordinated $ZnHis_3(H_2O)$, (*d*) four-coordinated $ZnHis_2Cl_2$, (*e*) four-coordinated $ZnHis_2(H_2O)_2$.

As seen from Table 4 and Figure 5, the best fits are generally obtained from the models (*b*)–(*e*) where zinc is four-coordinated with pseudo-tetrahedral geometry, and ligated by two or three histidine ligands. In accordance with the results from the XANES analysis, the six-coordinated Zn complex, model (*a*), which is the species present in the T_6 conformation of insulin does not fit the experimetal EXAFS spectra well, particularly at *k*-values around 4–5 $Å^{-1}$.

A model including a single histidine ligand was tested, but resulted in a bad fit with unrealistically low Debye-Waller factors compensating for the low histidine occupation. Species where zinc is ligated by two histidine residues as in models (*d*) and (*e*), have earlier been observed at a dimer-dimer interface of a hexamer in crystal structures of the T_3R_3 conformation of insulin(Smith et al., 2001) in which two symmetry-related HisB5 residues are involved. Reasonable fits were observed for both model (*d*) and (*e*), which included two histidine residues in the ligation. However, the models that best describes the histidine signature occurring at *k*-values around 4–5 $Å^{-1}$ are those with a Zn-ligation to three histidine ligands, models (*b*) and (*c*).

In general, the Debye-Waller factors in the fibril sample are higher compared to the values observed in crystalline insulin. This demonstrates that there is a higher thermal and/or static disorder around the zinc coordinated in fibrils compared to the Zn-coordination in crystals. However, for model (*d*) a significantly lower Debye-Waller factor was observed for the first shell and following high standard deviations were observed. This indicates an occupation number higher than 2 in the first radial shell around 2.0 Å from the zinc. In comparison, the parameters found by refinement of model (*e*) which includes two oxygen atoms with a distance around 2.0 Å from zinc, are more realistic than model (*d*) even though the *R*-factor for this fit is higher.

As shown in Figure 5 the amplitude of the modulation at 12 $Å^{-1}$ in the experimental EXAFS spectrum is quite high indicating coordination to heavier elements such as chlorine. This indication can be verified by the radial distribution, where the peak at distances around 2.2 Å, occurring as a shoulder to the high peak at 2.0 Å, is better modelled by those models containing chloride ions, i.e. models (*b*) and (*d*).

In conclusion, a zinc coordination analogue to that observed in R_6 insulin crystals where zinc is ligated by three histidine residues and one chloride ion provides the best fits with both the EXAFS as well as the XANES data, wherefore this coordination must be the most prominent for zinc in insulin fibrils even though other zinc coordination geometries may be present, as well. This is surprising since the R_6 insulin conformation normally occur in the presence of phenolic ligands and since insulin is shown to be far from in its native, mainly α-helical, structure when being incorporated into β-sheet-rich fibrils.

An analogue EXAFS analysis was carried out for the semi-matured insulin fibrils. Though a Zn-coordination with three histidine residues and one chloride ion similar to that found in the fully matured fibrils was shown to provide the best fit, this model was not sufficient to describe all the features, and it must be concluded that more coordination geometries of zinc are present in significant amounts. This is in agreement with the result from the XANES spectra, where a mixture of 78% tetra- and 22% hexa-coordinated zinc is found in the semi-matured fibrils.

The X-ray absorption spectroscopy analysis clearly demonstrates that zinc is incorporated in the fibrils where it coordinates to histidine residues, and most likely in a coordination environment similar to that observed in insulin R_6 hexamers.

Fibrillation of insulin

The output from typical fibrillation experiments are shown in Figure 6, in which the normalized ThT fluorescence intensity, which corresponds to the fraction of insulin converted into fibrils, is plotted as a function of time. In Figure 6*a* the normalized ThT fluorescence signal is fitted with a single step sigmoidal curve from which the lag time and apparent growth rate constants are determined. Some fibrillation experiments typically at temperatures below 45 ºC show a two-step process in which the two elongation steps are clearly distinguished. Such data were fitted by a double step sigmoidal curve, as shown in Figure 6*b*. In all data series, the growth rates for each of the two steps $k_{app,1}$ and $k_{app,2}$ are very close to each other both matching the value determined by the single step model, but the double step model highly improves the determination of the lag time. A two-step mechanism is also indicated in Figure 6*a*, but the fraction of fibril in the first elongation phase, x, is not high enough to obtain a robust fit.

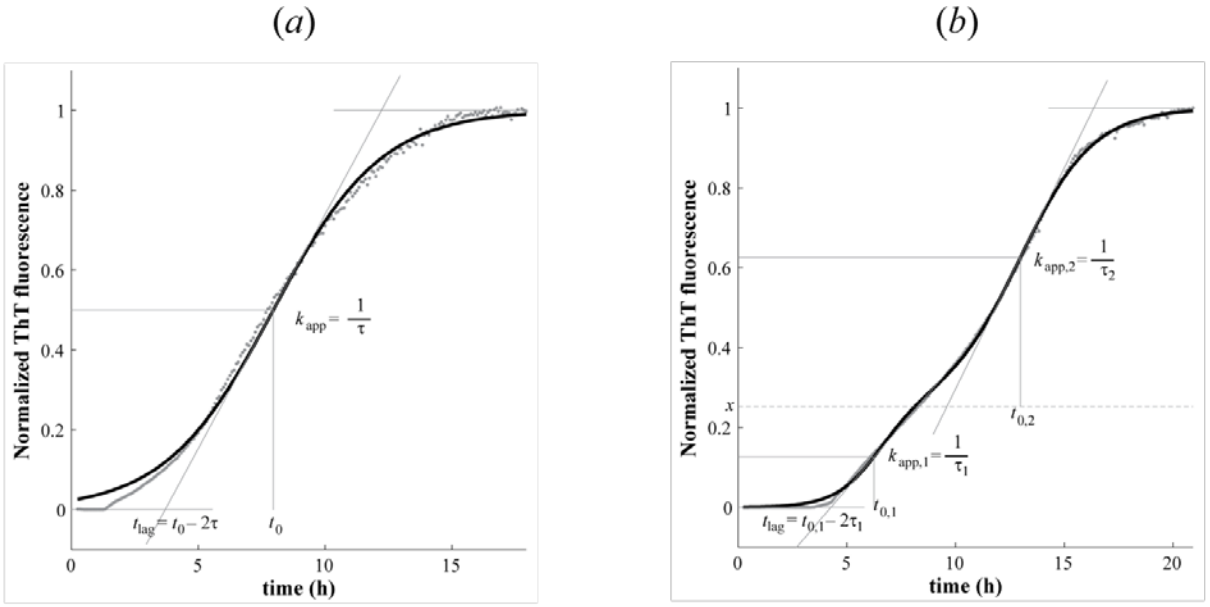

Figure 6: Normalized ThT fluorescence intensity measured during fibrillation of 2.0 mg ml^{-1} insulin at 45°C. (*a*) Without presence of Zn^{2+} the data were modelled by the single step sigmoidal model. (*b*) In presence of stoichiometric amounts of Zn^{2+} data were modelled by the double step sigmoidal model. The quantities t_{lag} and k_{app} determined from the fit are shown.

Hydroxylation of ThT, by which the dye loses its color, becomes important at pH > 7.3 (Foderà et al., 2008). As this study was carried out at pH 7.3 (which may by the maximum pH by which ThT can be used) small traces of ThT decay were observed in some of the samples. Though the decay is accelerated with increasing temperature, all fibrillation processes were completed within the absorbance decay times determined by Foderà *et al.* (Foderà et al., 2008).

Poor precision in the lag-time of the fibrillation process was observed particularly for the Zn-containing samples. Therefore, it was chosen to perform at least 10 replicates of each condition. However, for low concentration samples fibrillated at low temperatures it was furthermore necessary to perform even more repetitions in order to ensure good statistics. This indicates that formation of fibril nuclei is a spontaneous process, which becomes even more incontrollable at low concentrations and low temperatures.

The influence of insulin concentration

The average lag time and apparent growth rates for fibrillation at 45°C at different concentrations are listed in Table 5. Presence of Zn^{2+} generally increases the lag time, but it also increases the standard deviations, which seems to be a general trend. The lag time values of fibrillation without Zn^{2+} are in good agreement with insulin

fibrillation at pH 1.6 (Nielsen et al., 2001b), whereas in presence of Zn^{2+} increasing lag times were observed with increasing concentrations except at very low concentrations, where a high lag time was observed possibly due to long distance between the reactants. The apparent fibrillation rate decreases with increasing concentrations, which is in agreement with Noormägi *et al.* (Noormägi et al., 2010). However, no large variations were observed between presence and absence of Zn^{2+}.

Table 5: Lag time and apparent growth rates of fibrillation at different insulin concentrations. Standard deviations are stated in parentheses.

	Zn-free samples		Zn containing samples	
Insulin conc. (mg ml^{-1})	t_{lag}	k_{app}	t_{lag}	k_{app}
0.02	6.9 (1.1)	8.6 (1.3)	16.7 (6.6)	7.2 (1.7)
0.2	2.0 (0.5)	2.2 (0.5)	3.8 (1.8)	1.3 (0.2)
2.0	3.2 (0.6)	0.46 (0.08)	4.1 (1.4)	0.41 (0.04)
10	3.0 (0.5)	0.67 (0.08)	19.3 (2.7)	0.24 (0.01)

The influence of temperature

The dependence of temperature on the lag time is shown in Figure 7 for three different insulin concentrations. It is seen that in presence of Zn^{2+}, the lag time decreases with increasing temperature for all concentrations studied. For temperatures below 45 ºC, in particular, presence of Zn^{2+} highly increases the lag time compared to samples without Zn^{2+}, but it also increases the standard deviations. In absence of Zn^{2+} the lag time is less dependent on temperature, except at insulin concentration of 0.02 mg ml^{-1} (Figure 7*a*).

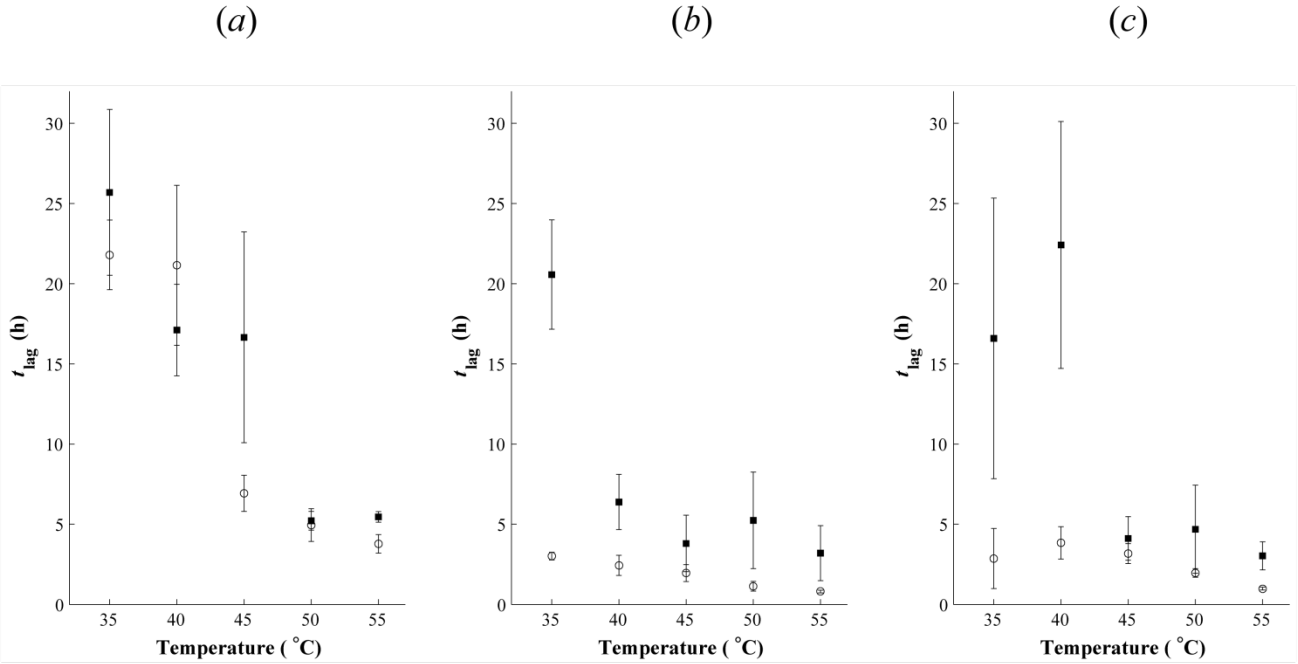

Figure 7: Lag time plotted as function of the temperature for different insulin concentrations (*a*) 0.02 mg ml^{-1}, (*b*) 0.2 mg ml^{-1}, and (*c*) 2 mg ml^{-1}. Zn-free (open circles), in presence of stoichiometric amounts of Zn (filled squares).

The temperature dependence of the apparent fibrillation growth rate of different insulin concentration with and without presence of Zn^{2+} is shown as Arrhenius plots in Figure 8. In presence of Zn^{2+}, the enthalpy of activation E_a seems to some extent to be independent of concentration, whereas for the zinc-free samples an increasing E_a is observed with increasing insulin concentration. In accordance with the previous results the fibrillation process is more spontaneous and incontrollable at low concentrations (0.02 mg ml^{-1}) due to the long distances between the reactants, wherefore higher standard deviations of the activation enthalpy are observed.

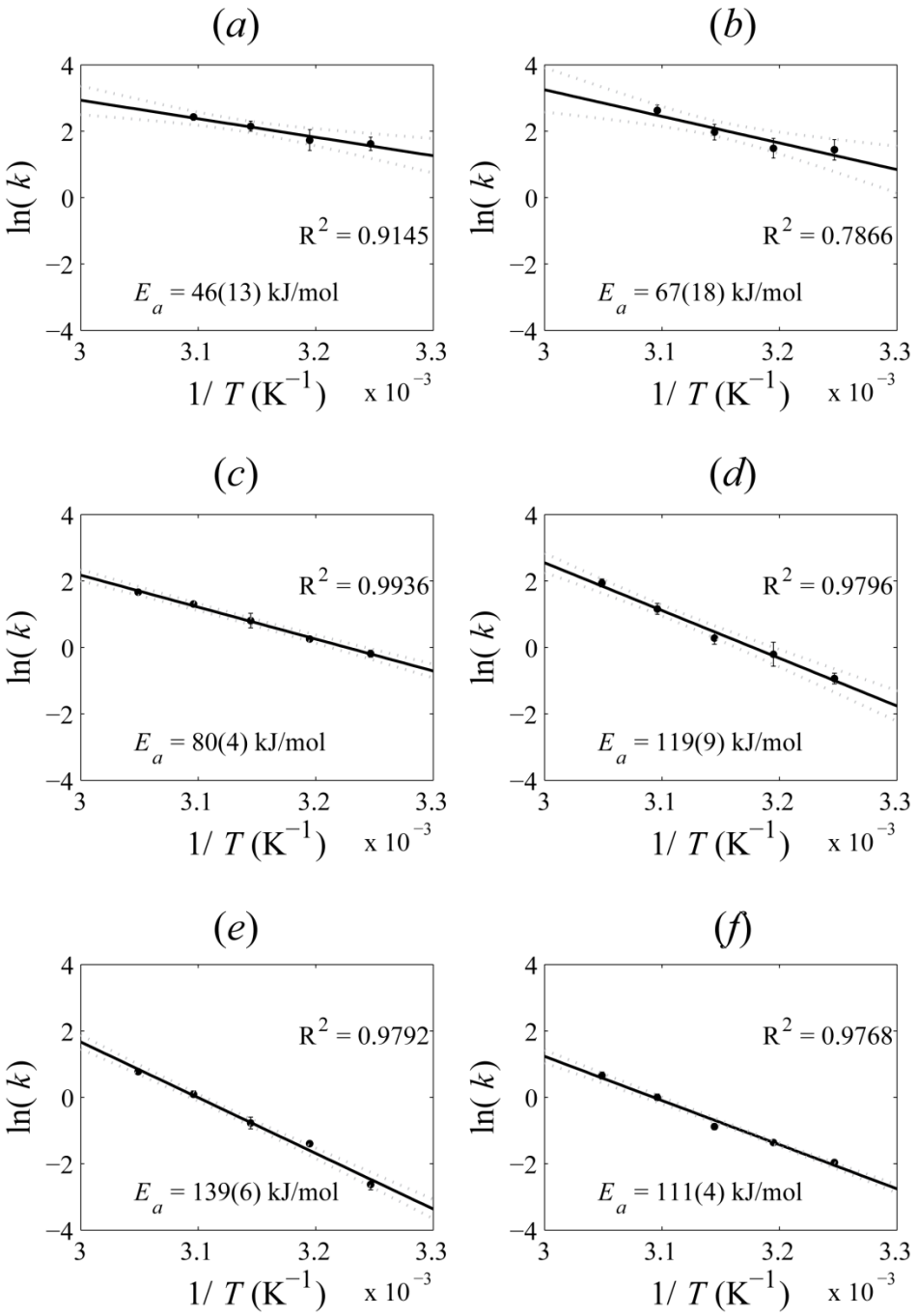

Figure 8: Arrhenius plots showing the temperature dependence of the apparent fibrillation growth rate of different insulin concentration, 0.02 mg ml^{-1} (top panel), 0.2 mg ml^{-1} (middle panel), 2.0 mg ml^{-1} (bottom panel). Zn-free (left column), fibrillation in presence of Zn^{2+} (right column). The 95 % confidence intervals of the linear regression from which the enthalpies of activation E_a are calculated are shown as dashed lines. The standard deviation of E_a is denoted in parentheses. The goodness of fit is evaluated by the coefficient of determination R^2.

Fibrillation at 35°C was slow particularly at high concentrations where completion could take up to three days. Conversely, at low insulin concentration the fibril growth was completed within 15 minutes after termination of the lag phase at 55°C, meaning that the fibrillation growth is recorded by only a few data points with the current setup. Therefore, only 35–50°C data are included in the 0.02 mg ml^{-1} series.

Discussion

It has been long known that zinc ions hamper the fibrillation of insulin. Thus, most models on insulin fibrillation take their offset in the insulin monomer – without zinc bound. Using X-ray absorption spectroscopy we have investigated zinc binding in insulin fibrils and compared the kinetics of fibril formation with and without the presence of zinc. The experiments have been performed at pH 7.3, where we know that zinc can bind to the histidine ligands, which at this pH is partly deprotonated.

We checked the oligomerization of insulin at the initial stage of the experiment using SAXS. In the presence of zinc, we observed insulin solely in the hexameric form. As the buffer does not contain phenol or anything else that can force the system into the R_6 conformation, this hexamer adopts the T_6 conformation, which was also verified by SAXS. Without the presence of zinc we observed a concentration dependent equilibrium between dimeric and hexameric insulin. At low concentration (1 mg/mL) 77 % was in the dimeric form while at the higher concentration (10 mg/mL) only 51 % was in the dimeric form. SAXS data (Vestergaard et al., 2007) cannot be obtained at the very low concentrations so it is mere speculation that at the very low concentration (0.02 mg /mL) we primarily have insulin in the dimeric form or even in the monomeric form.

Fibril morphology

Zinc is apparently inferring somewhat with the morphology of the fibrils. TEM measurements shown in Fig. 2 clearly show that the zinc containing fibrils in Fig. 2*a* are similar to the zinc-free fibrils shown in Fig. 2*b* but according to the size distribution they appear to be larger and less frayed when zinc is bound. A comparison with the fibrils made at pH 2.0, shown in Fig. 2*c* shows that pH indeed has a large impact on the fibril morphology. pH 2.0 is below pI of histidine so that zinc is not coordinated, but furthermore at pH 2.0 insulin is present primarily as monomers (Vestergaard et al., 2007), meaning that the starting point of the fibril formation is quite different at this pH.

Despite the lack of an overall elongated structure detected by TEM for the fibrils formed at pH 7.3, we confirmed the fibrillar nature of the samples using fibre diffraction, binding to the dye ThT and a growth kinetics resembling traditional fibrillation kinetics. The performed diffraction experiment of the fibrils clearly gave diffraction at 4.7 Å and a weaker signal at approximately 11 Å. The signal at 4.7 Å is due to the distance between β-strands in a β-sheet and the weaker signal at 11 Å is due to the distance between the individual beta sheets. The presence of these signals is generally recognized to be an indicator of fibrillation. Clearly the fibrils formed at pH 2.0 are more

elongated and were therefore easier to align which is also reflected in the fibre diffraction patterns in figure 1, where 1c and to some extend 1a have a better alignment of the fibrils than the data in figure 1b where the signal is more disordered. Different fibril morphologies is also seen for glucagon (Ghodke et al., 2012).

Zinc coordination

Following the fibrillation process using ThT assay we collected samples from semi-matured and from matured samples. We pooled the fibrillated insulin, washed with zinc-free buffer and collected XAS spectra. Several samples were tested and our measurements clearly showed that zinc binds to the fibrillated insulin. Comparison to the XAS spectra from crystalline samples of insulin in respectively the T_6 and the R_6 forms, shown in Fig. 4, showed that the semi-matured insulin fibrils bind zinc somewhere in between the T_6 and R_6 form and the fully matured fibrils bind zinc in a form very similar to the R_6 form. In the R_6 form, zinc is tetra-coordinated with three histidine ligands and one chloride ligand. This seriously suggests that the zinc ions stay coordinated by the tree histidine residues when they are stressed, but that the zinc-binding site is going from a more open T_6 site to a more closed R_6 site upon fibrillation of insulin.

Fibrillation kinetics

Furthermore, we have followed the kinetics of the fibril formation with and without zinc at 45 ºC. We can confirm earlier results (J Brange et al., 1997) that the presence of zinc generally impedes the fibril formation seen as a longer lag-time. It is also clear that when the fibrillation process has started, the presence of zinc seems to be insignificant. This is seen in Table 2. and Fig. 7 where the lag-time is clearly different for the two types of experiments but the apparent rate constant are seen to be almost identical.

Finally, we have investigated the influence of temperature. The Arrhenius plots are indeed difficult to make as it appears that some of the fibrillation curves are two-step like and some of the fibrillation curves are one-step like. What is apparent from Fig. 8 is that for the zinc-free measurement the enthalpy of activation E_a is increasing with protein concentration and that for the zinc-containing samples the enthalpy of activation is more or less independent of the protein concentration.

Our results are in somewhat accordance with the results seen from hIAPP, where zinc is also seen to coordinate a histidine residue and thereby impede the fibril formation at low hIAPP concentrations but where zinc is speeding

up the fibril formation at higher hIAPP concentrations (Brender et al., 2010). Apart from the zinc dependence of hIAPP fibrillation it has also been suggested that monomeric insulin inhibits hIAPP amyloid fibrillation by forming an insulin:hIAPP heterodimer (Wiltzius et al., 2009). The interplay between the three: zinc, insulin, and hIAPP must in indeed be a very delicate equilibrium.

Fibrillation mechanism

Due to the different morphologies - frayed or not frayed, the fact that zinc binds in the insulin fibrils and the different temperature dependencies on the enthalpies of activation lead us to suggest that the structure of the fibril nucleus could be different depending on whether the starting insulin is hexamers or dimers. Having said that we still realize that considerable refolding of the insulin – either in hexamer or in dimer – need to happen for fibrillation to occur. The different building blocks then lead to different morphologies, which is observed in the TEM pictures. If the fibrillation primarily comes from hexamers these are stabilized by the zinc ions – even at lower concentrations - and therefore the enthalpy of activation is independent of the protein concentration. If zinc is not part of the buffer, an equilibrium between hexamers and dimers will be sustained, which will go towards dimers for lower protein concentrations. Assuming that dimers fibrillate faster than hexamers will then give the apparent change in enthalpy of activation seen in Fig. 8.

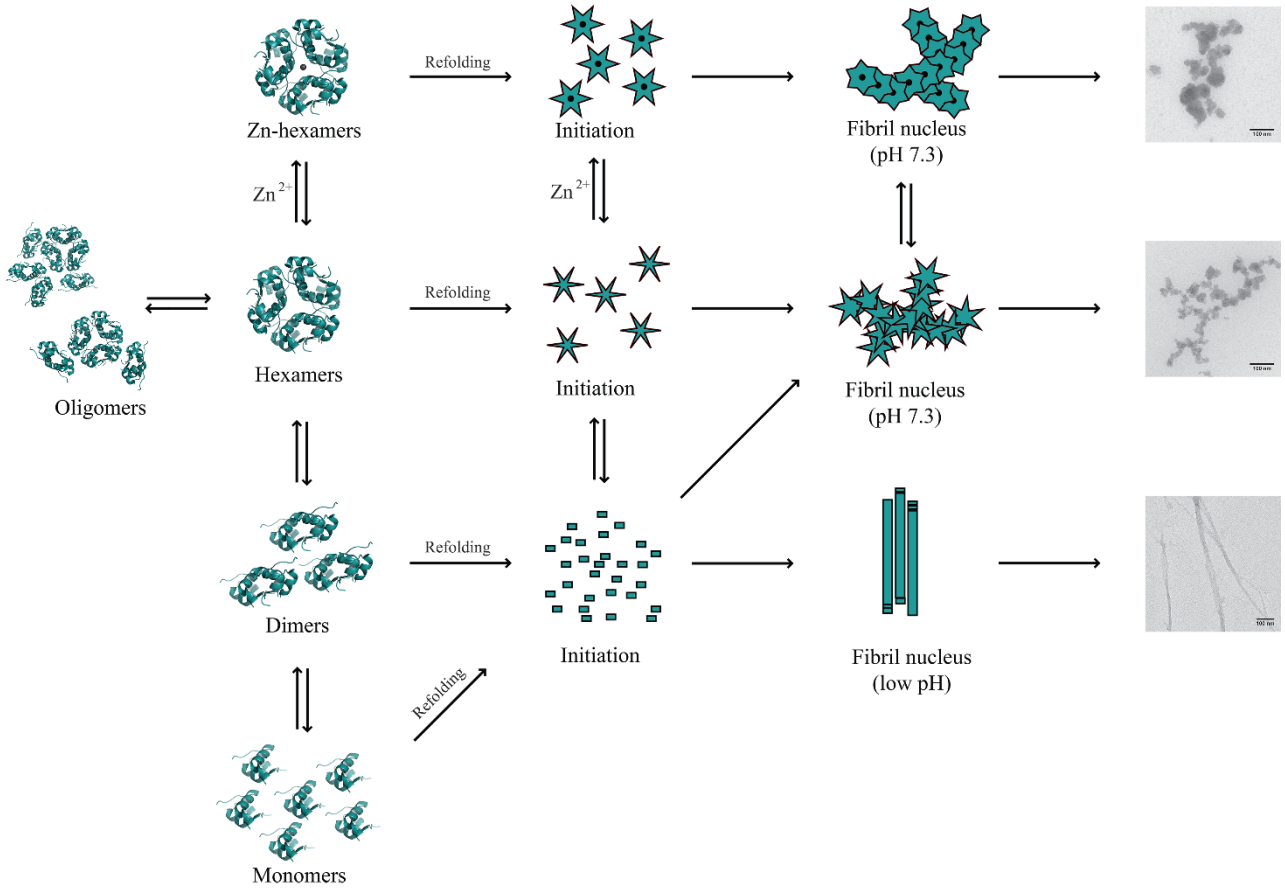

Figure 9: Proposed mechanism of fibrillation at low pH and pH = 7.3.

Conclusion

We have investigated fibrillation of insulin in the present of zinc and compared to results without the presence of zinc. In agreement with other studies (Jens Brange et al., 1997a; Nielsen et al., 2001a), our study clearly shows that zinc indeed influences the kinetics and the morphology of the fibrils. It also shows that zinc incorporates in the fibrils and coordinates to histidine residues in an environment, which is similar to the coordination seen in the insulin R_6 hexamers, where three histidine residues and a chloride ion is coordinating the zinc.

Acknowledgements

Portions of this research were carried out at beamlines I811 and I911, MAX-lab synchrotron radiation source, Lund University, Sweden. Funding for the beamline I811 project was kindly provided by The Swedish Research Council and The Knut och Alice Wallenbergs Stiftelse. The research presented has received funding from DANSCATT (the Danish agency and for Science, Technology and Innovation).

References

Ahmad, A., Millett, I.S., Doniach, S., Uversky, V.N., Fink, A.L., 2004. Stimulation of Insulin Fibrillation by Urea-induced Intermediates. J. Biol. Chem. 279, 14999–15013. doi:10.1074/jbc.M313134200

Ahmad, A., Millett, I.S., Doniach, S., Uversky, V.N., Fink, A.L., 2003. Partially folded intermediates in insulin fibrillation. Biochemistry 42, 11404–11416. doi:10.1021/bi034868o

Andra, N., Gavrilova, J., Smirnova, J., Tougu, V., Palumaa, P., 2010. Zn(II) Ions Inhibit Fibrillization of Monomeric Insulin. FEBS J. 277, 256–257.

Baker, E.N., Blundell, T.L., Cutfield, J.F., Cutfield, S.M., Dodson, E.J., Dodson, G.G., Hodgkin, D.M., Hubbard, R.E., Isaacs, N.W., Reynolds, C.D., 1988. The structure of 2Zn pig insulin crystals at 1.5 A resolution. Philos. Trans. R. Soc. Lond. B. Biol. Sci. 319, 369–456. doi:10.1098/rstb.1988.0058

Binsted, N., Campbell, J.W., Gurman, S.J., Stephenson, P.C., 1991. EXCURV92. SERC, Daresbury Laboratory, Warrington.

Binsted, N., Strange, R.W., Hasnain, S.S., 1992. Constrained and restrained refinement in EXAFS data analysis with curved wave theory. Biochemistry 31, 12117–12125.

Bordas, J., Dodson, G.G., Grewe, H., Koch, M.H.J., Krebs, B., Sir Randall, J., 1983. A Comparative Assessment of the Zinc--Protein Coordination in 2Zn--Insulin as Determined by X-ray Absorption Fine Structure (EXAFS) and X-ray Crystallography. Proc. R. Soc. B Biol. Sci. 219, 21–39. doi:10.1098/rspb.1983.0056

Brange, J., Andersen, L., Laursen, E.D., Meyn, G., Rasmussen, E., 1997. Toward understanding insulin fibrillation. J. Pharm. Sci. 86, 517–525. doi:10.1021/js960297s

Brange, J., Andersen, L., Laursen, E.D., Meyn, G., Rasmussen, E., 1997a. Toward understanding insulin fibrillation. J. Pharm. Sci. 86, 517–525. doi:10.1021/js960297s

Brange, J., Havelund, S., Hommel, E., Sorensen, E., Kuhl, C., 1986. Neutral Insulin Solutions Physically Stabilized by Addition of Zn-2+. Diabet. Med. 3, 532–536.

Brange, J., Whittingham, J., Edwards, D., You-Shang, Z., Wollmer, A., Brandenburg, D., Dodson, G., Finch, J., 1997b. Insulin structure and diabetes treatment. Curr. Sci. 72, 470–476.

Brender, J.R., Hartman, K., Nanga, R.P.R., Popovych, N., de la Salud Bea, R., Vivekanandan, S., Marsh, E.N.G., Ramamoorthy, A., 2010. Role of Zinc in Human Islet Amyloid Polypeptide Aggregation. J. Am. Chem. Soc. 132, 8973–8983. doi:10.1021/ja1007867

Carlson, S., Clausén, M., Gridneva, L., Sommarin, B., Svensson, C., 2006. XAFS experiments at beamline I811, MAX-lab synchrotron source, Sweden. J. Synchrotron Radiat. 13, 359–64. doi:10.1107/S0909049506025611

Ciszak, E., Smith, G.D., 1994. Crystallographic Evidence for Dual Coordination around Zinc in the T3R3 Human Insulin Hexamer. Biochemistry 33, 1512–1517.

Coffman, F.D., Dunn, M.F., 1988. Insulin-metal ion interactions: the binding of divalent cations to insulin hexamers and tetramers and the assembly of insulin hexamers. Biochemistry 27, 6179–6187. doi:10.1021/bi00416a053

Diao, J., 2003. Crystallographic titration of cubic insulin crystals: pH affects GluB13 switching and sulfate binding. Acta Crystallogr. D Biol. Crystallogr. 59, 670–676. doi:10.1107/S0907444903002208

Dische, F.E., Wernstedt, C., Westermark, G.T., Westermark, P., Pepys, M.B., Rennie, J.A., Gilbey, S.G., Watkins, P.J., 1988. Insulin as an Amyloid-Fibril Protein at Sites of Repeated Insulin Injections in a Diabetic Patient. Diabetologia 31, 158–161. doi:10.1007/BF00276849

Domigan, L.J., Healy, J.P., Meade, S.J., Blaikie, R.J., Gerrard, J.A., 2012. Controlling the dimensions of amyloid fibrils: toward homogenous components for bionanotechnology. Biopolymers 97, 123–33. doi:10.1002/bip.21709

Feiters, M.C., Eijkelenboom, A.P., Nolting, H.F., Krebs, B., van den Ent, F.M., Plasterk, R.H., Kaptein, R., Boelens, R., 2003. X-ray absorption spectroscopic studies of zinc in the N-terminal domain of HIV-2 integrase and model compounds. J. Synchrotron Radiat. 10, 86–95.

Foderà, V., Groenning, M., Vetri, V., Librizzi, F., Spagnolo, S., Cornett, C., Olsen, L., van de Weert, M., Leone, M., 2008. Thioflavin T hydroxylation at basic pH and its effect on amyloid fibril detection. J. Phys. Chem. B 112, 15174–81. doi:10.1021/jp805560c

Frankr, C.G., Harris, P., Ståhl, K., 2011. A sample holder for in-house X-ray powder diffraction studies of protein powders. J. Appl. Crystallogr. 44, 1288–1290. doi:10.1107/S0021889811039057

Frankær, C.G., Knudsen, M. V, Norén, K., Nazarenko, E., Ståhl, K., Harris, P., 2012. The Structures of T6, T3R3 and R6 Bovine Insulin: Combining X-ray Diffraction and Absorption Spectroscopy. Acta Crystallogr. D, Biol. Crystallogr. 68, 1259–1271. doi:10.1107/S090744491202625X

Gasteiger, E., 2003. ExPASy: the proteomics server for in-depth protein knowledge and analysis. Nucleic Acids Res. 31, 3784–3788. doi:10.1093/nar/gkg563

Gasteiger, E., Hoogland, C., Gattiker, A., Duvaud, S., Wilkins, M.R., Appel, R.D., Bairoch, A., 2005. Protein Identification and Analysis Tools on the ExPASy Server, The Proteomics Protocols Handbook. Humana Press Inc., Totowa.

Ghodke, S., Nielsen, S.B., Christiansen, G., Hjuler, H.A., Flink, J., Otzen, D., 2012. Mapping out the multistage fibrillation of glucagon. FEBS J. 279, 752–65.

Groenning, M., 2010. Binding mode of Thioflavin T and other molecular probes in the context of amyloid fibrils-current status. J. Chem. Biol. doi:10.1007/s12154-009-0027-5

Groenning, M., Frokjaer, S., Vestergaard, B., 2009. Formation mechanism of insulin fibrils and structural aspects of the insulin fibrillation process. Curr. Protein Pept. Sci. 10, 509–528.

Gurman, S.J., Binsted, N., Ross, I., 1986. A rapid, exact, curved-wave theory for EXAFS calculations. II. The multiple-scattering contributions. J. Phys. C Solid State Phys. 19, 1845–1861.

Gurman, S.J., Binsted, N., Ross, I., 1984. A RAPID, EXACT CURVED-WAVE THEORY FOR EXAFS CALCULATIONS. J. Phys. C - solid state Phys. 17, 143–151. doi:10.1088/0022-3719/17/1/019

Inada, Y., Hayashi, H., Sugimoto, K., Funahashi, S., 1999. Solvation Structures of Manganese(II), Iron(II), Cobalt(II), Nickel(II), Copper(II), Zinc(II), and Gallium(III) Ions in Methanol, Ethanol, Dimethyl Sulfoxide, and Trimethyl Phosphate As Studied by EXAFS and Electronic Spectroscopies. J. Phys. Chem. A 103, 1401–1406. doi:10.1021/jp983799y

Konarev, P. V., Volkov, V. V., Sokolova, A. V., Koch, M.H.J., Svergun, D.I., 2003. PRIMUS : a Windows PC-based system for small-angle scattering data analysis. J. Appl. Crystallogr. 36, 1277–1282.

Krebs, M.R., Domike, K.R., Cannon, D., Donald, A.M., 2008. Common motifs in protein self-assembly. Faraday Discuss. 139, 265–274.

Kurouski, D., Dukor, R.K., Lu, X., Nafie, L.A., Lednev, I.K., 2012. Normal and reversed supramolecular chirality of insulin fibrils probed by vibrational circular dichroism at the protofilament level of fibril structure. Biophys. J. 103, 522–31. doi:10.1016/j.bpj.2012.04.042

Kaarsholm, N.C., Ko, H.C., Dunn, M.F., 1989. Comparison of Solution Structural Flexibility and Zinc Binding Domains for Insulin, Proinsulin, and Miniproinsulin. Biochemistry 28, 4427–4435.

Labrador, A., Cerenius, Y., Svensson, C., Theodor, K., Plivelic, T., 2013. The yellow mini-hutch for SAXS experiments at MAX IV Laboratory. J. Phys. Conf. Ser. 425, 072019. doi:10.1088/1742-6596/425/7/072019

Levine, H., 1995. Thioflavine T Interaction with Amyloid β-Sheet Structures. Amyloid Int. J. Exp. Clin. Investig. 2, 1–6.

Levine, H., 1993. Thioflavine T Interaction with Synthetic Alzheimer's Disease β-Amyloid Peptides: Detection of Amyloid Aggregation in Solution. Protein Sci. 2, 404–410.

Librizzi, F., Rischel, C., 2005. The kinetic behavior of insulin fibrillation is determined by heterogeneous nucleation pathways. Protein Sci. 14, 3129–3134. doi:10.1110/ps.051692305

Nayak, A., Sorci, M., Krueger, S., Belfort, G., 2009. A universal pathway for amyloid nucleus and precursor formation for insulin. Proteins 74, 556–565. doi:10.1002/prot.22169; 10.1002/prot.22169

Nielsen, L., Frokjaer, S., Brange, J., Uversky, V.N., Fink, A.L., 2001a. Probing the mechanism of insulin fibril formation with insulin mutants. Biochemistry 40, 8397–8409.

Nielsen, L., Frokjaer, S., Carpenter, J.F., Brange, J., 2001b. Studies of the structure of insulin fibrils by Fourier transform infrared (FTIR) spectroscopy and electron microscopy. J. Pharm. Sci. 90, 29–37.

Nielsen, L., Khurana, R., Coats, A., Frokjaer, S., Brange, J., Vyas, S., Uversky, V.N., Fink, A.L., 2001c. Effect of environmental factors on the kinetics of insulin fibril formation: elucidation of the molecular mechanism. Biochemistry 40, 6036–6046.

Noormägi, A., Gavrilova, J., Smirnova, J., Tõugu, V., Palumaa, P., 2010. Zn(II) ions co-secreted with insulin suppress inherent amyloidogenic properties of monomeric insulin. Biochem. J. 430, 511–518. doi:10.1042/BJ20100627; 10.1042/BJ20100627

Patel, H.R., Pithadia, A.S., Brender, J.R., Fierke, C.A., Ramamoorthy, A., 2014. In Search of Aggregation Pathways of IAPP and Other Amyloidogenic Proteins: Finding Answers through NMR Spectroscopy. J. Phys. Chem. Lett. 5, 1864–1870. doi:10.1021/jz5001775

Petoukhov, M. V., Franke, D., Shkumatov, A. V., Tria, G., Kikhney, A.G., Gajda, M., Gorba, C., Mertens, H.D.T., Konarev, P. V., Svergun, D.I., 2012. New developments in the ATSAS program package for small-angle scattering data analysis. J. Appl. Crystallogr. 45, 342–350.

Podestà, A., Tiana, G., Milani, P., Manno, M., 2006. Early events in insulin fibrillization studied by time-lapse

atomic force microscopy. Biophys. J. 90, 589–597. doi:10.1529/biophysj.105.068833

Ressler, T., 1998. WinXAS: a program for X-ray absorption spectroscopy data analysis under MS-Windows. J. Synchrotron Radiat. 5, 118–122. doi:10.1107/S0909049597019298

Sluzky, V., Tamada, J.A., Klibanov, A.M., Langer, R., 1991. Kinetics of insulin aggregation in aqueous solutions upon agitation in the presence of hydrophobic surfaces. Proc. Natl. Acad. Sci. U. S. A. 88, 9377–9381.

Smith, G.D., Pangborn, W.A., Blessing, R.H., 2005. The Structure of T6 Bovine Insulin. Acta Crystallogr. D Biol. Crystallogr. 61, 1476–1482.

Smith, G.D., Pangborn, W.A., Blessing, R.H., 2003. The Structure of T6 Human Insulin at 1.0 Å Resolution. Acta Crystallogr. D Biol. Crystallogr. 59, 474–482.

Smith, G.D., Pangborn, W.A., Blessing, R.H., 2001. Phase changes in T(3)R(3)(f) human insulin: temperature or pressure induced? Acta Crystallogr. D Biol. Crystallogr. 57, 1091–100. doi:10.1107/S0907444901007685

Storkel, S., Schneider, H.M., Muntefering, H., Kashiwagi, S., 1983. Iatrogenic, Insulin-Dependent, Local Amyloidosis. Lab. Investig. 48, 108–111.

Svergun, D., Barberato, C., Koch, M.H., 1995. CRYSOL - A program to evaluate X-ray solution scattering of biological macromolecules from atomic coordinates. J. Appl. Crystallogr. 28, 768–773. doi:10.1107/S0021889895007047

Vestergaard, B., Groenning, M., Roessle, M., Kastrup, J.S., van de Weert, M., Flink, J.M., Frokjaer, S., Gajhede, M., Svergun, D.I., 2007. A helical structural nucleus is the primary elongating unit of insulin amyloid fibrils. PLoS Biol. 5, 1089–1097. doi:10.1371/journal.pbio.0050134

Waugh, D.F., 1944. The Linkage of Corpuscular Protein Molecules. I. A Fibrous Modification of Insulin. J. Am. Chem. Soc. 66, 663.

Wiltzius, J.J.W., Sievers, S.A., Sawaya, M.R., Eisenberg, D., 2009. Atomic structures of IAPP (amylin) fusions suggest a mechanism for fibrillation and the role of insulin in the process. Protein Sci. 18, 1521–1530. doi:10.1002/pro.145

Zitolo, A., D'Angelo, P., 2010. X-ray absorption spectroscopy study of the solvation structure of zinc(II) in dimethyl sulfoxide solution. Chem. Phys. Lett. 499, 113–116. doi:10.1016/j.cplett.2010.09.034